Numerical evaluation of heat/mass transfer analogy for leading edge showerhead film cooling on a first-stage vane

Silvia Ravelli*, Giovanna Barigozzi

Department of Engineering and Applied Sciences, University of Bergamo, Marconi St. 5, 24044 Dalmine, Italy

silvia.ravelli@unibg.it, giovanna.barigozzi@unibg.it

* Corresponding author: silvia.ravelli@unibg.it, Tel: +39 035 2052346, Fax: +39 035 2052077.

Abstract

A numerical study was conducted to evaluate the applicability of the heat/mass transfer analogy to leading edge film cooling on a first-stage vane. A typical showerhead configuration was taken into account, thus including four staggered rows of evenly spaced cylindrical holes, angled at 45° towards the tip. The investigation was carried out at low speed (isentropic exit Mach number of Ma_{2is} = 0.2), inlet turbulence intensity of Tu_1 = 1.6% and 13%, and three different blowing ratios (*BR* = 2.0, 3.0 and 4.0). Steady-state simulations were conceived to mimic the pressure sensitive paint (PSP) technique aiming to measure the adiabatic film cooling effectiveness (η) in the leading edge region, under a density ratio of *DR* = 1 and 1.5. With the mainstream flow assumed to be air at ambient temperature, the desired *DR* was obtained by injecting coolant as air at different temperature from the mainstream (namely, heat transfer approach) or as isothermal foreign gas (namely, mass transfer approach). Despite the dominant effect of the *DR* on η, results indicated that the heat/mass transfer properties of the coolant are to be considered when comparing film cooling performance, at matched *BR* conditions. At low inlet turbulence intensity, the heat/mass transfer analogy was found to be applicable only to the lowest *BR* of 2.0. Its validity was extended to the medium *BR* of 3.0, in case of *DR* = 1.5, provided that the leading edge is approached by high turbulence intensity flow.

Keywords: Gas turbine, Film cooling, Showerhead, Heat/mass transfer, CFD modeling

1. Introduction

The leading edge of a turbine vane is subjected to some of the highest thermal loading within a gas turbine engine. Since turbine airfoils are optimized for aerodynamic performance and heat load to improve airfoil durability, a deep understanding of the leading edge flow is essential when designing an efficient turbine. Typically, blunt leading edges are conceived to minimize heat transfer at the stagnation point, together with showerhead arrangement [1]. The external heat transfer actually depends on the development of the boundary layer whose behavior is strongly affected by the presence of film cooling jets, temperature and pressure gradients, flow unsteadiness and turbulence, as well as separation bubbles near the airfoil leading edge. A lot of research has been done to measure the vane surface temperature at the leading edge region with different showerhead geometrical features, including the shape of the holes

(cylindrical vs. fan shaped ones), their arrangement (number of rows, number of holes in each row, hole spacing) and inclination to the surface. The test matrix is complicated by the external flow conditions (mainstream Mach number and Reynolds number, turbulence intensity) and the showerhead blowing conditions, commonly defined by the density ratio (*DR*), velocity ratio (*VR*), blowing ratio (BR) and the momentum flux ratio (*I*):

$$DR = \frac{\rho_c}{\rho_\infty} \quad (1)$$

$$VR = \frac{U_c}{U_\infty} \quad (2)$$

$$BR = \frac{\rho_c U_c}{\rho_\infty U_\infty} \quad (3)$$

$$I = \frac{\rho_c U_c^2}{\rho_\infty U_\infty^2} \quad (4)$$

Two main issues arise in measuring film cooling effectiveness (η) at the leading edge. On the one hand, the experimental technique may affect the values of η that are measured. In fact, η levels determined by thermal methods, such as infrared thermography (IR) or liquid crystal, were found to be higher than those obtained by means of the mass-transfer analogy method [2-5]. The reason is that thermal methods suffer from conduction effects. Moreover, the validity of the heat-mass transfer analogy for η measurements requires that the turbulent Lewis number (Le_t) be approximately equal to 1, based on the landmark work by Jones [6]. Recently, Han, and Rallabandi [7] pointed out that $Le_t \sim 1$ implies that the flow is highly turbulent. This assumption might not be valid in the leading edge region where the flow is either laminar or intermittent, even in the presence of film cooling jets. On the other hand, the implementation of heat transfer tests under engine-like conditions in terms of coolant-to-mainstream temperature ratio is very difficult. So laboratory experiments are commonly run under small temperature differences or isothermal conditions, with dense foreign gas simulating the coolant-to-mainstream density ratio which exists in a real engine. Accordingly, the application of PSP for determining η in the leading edge region is growing in popularity [8, 10], despite the above mentioned outstanding issues.

To know more about this fairly new technique, detailed uncertainty analysis has been performed to evaluate the effects of various uncertainties in PSP measurements on the distribution of η over the surface of interest [11, 12]: the main outcome consisted in experimental procedures or guidelines to achieve high-accuracy η measurements. Instead, Wiese et al. [13] focused on the suitability of the heat-mass transfer analogy when employing PSP to portray leading edge film cooling. They experimentally examined the efficacy of the PSP technique as a substitute for thermal IR measurements, using various coolant gases. Surprisingly, PSP was found to overpredict the film cooling performance as compared to

IR, even though the foreign gas (argon or nitrogen) maintained *Le* near unity. Moreover, they introduced the advective capacity ratio (ACR) defined as

$$ACR = \frac{\rho_c c_{P,c} U_c}{\rho_\infty c_{p,\infty} U_\infty} \qquad (5)$$

to account for the amount of thermal energy that the coolant can absorb from the mainstream, in addition to the traditional film cooling scaling parameters.

In the present work, the influence of coolant properties on leading film cooling has been examined through the use of different foreign gases (nitrogen and carbon dioxide). The computational approach was used to supplement the experimental investigation reported in [14], where η measurements in the leading edge region of a realistic, high pressure vane were performed using Binary PSP at *DR* values of about 1 and 1.5, matching either *BR* or *I*. The appropriate scaling parameter is another open question for the showerhead region: adiabatic effectiveness scaled with mass flux ratio for low blowing conditions and with *I* for high blowing conditions according to Ethridge et al. [15]. Cutbirth and Bogard [16] found that *I* is not a scaling parameter in between the showerhead rows of holes whereas it works properly downstream of the first row of holes on the vane pressure side. But progressing downstream along the pressure side, η was not scaled with either *BR* or *I*. Moreover, they put in evidence that scaling of pressure side film cooling is strongly dependent on the mainstream turbulence level. When dealing with computational fluid dynamics (CFD) modelling, numerical studies discussing whether or not *BR* and *I* properly account for the *DR* effects on the leading edge heat transfer, are currently very few and based on simplified geometries: Rutledge and Polanka [17] as well as Beirnaert-Chartrel and Bogard [18] simulated a quarter cylinder coupled with a flat afterbody, with a single coolant hole or three rows of holes, respectively. Results from [17, 18] indicated that *I* allows for the most accurate matching of coolant distribution and heat transfer coefficient augmentation due to film cooling whereas *BR* represents more precisely the location of the peak η value.

Whatever the scaling parameter, *BR* or *IR*, CFD simulations have been used here to assess the capability of the thermal and mass transfer approaches to predict showerhead film cooling in the leading edge region: the desired *DR* was obtained through temperature differences between the coolant and mainstream flows, in the former case, or by injecting foreign gas, at isothermal conditions, in the latter case. The two methods were compared by assessing differences in the computed local and laterally averaged values of η, for a given *BR*. A discussion on the validity of heat/mass transfer analogy in the context of complex interaction between multiple coolant rows and holes, represents an original contribution to current knowledge. Indeed, turbulent heat and mass diffusivities were experimentally investigated in simple flow cases, such as zero pressure gradient laminar/turbulent boundary layer over a flat plate [19, 20], or turbulent separated flow behind a backward facing step [21]. Han and Goldstein raised the bar in the field of turbomachinery:

they examined the validity of the heat/mass transfer analogy on a turbine blade [22] and endwall [23], but without film cooling. However, some evidence from [22] deserves a mention: when comparing heat and mass transfer data with $Nu/(Re_x^{0.5} Pr^n)$ and $Sh/(Re_x^{0.5} Sc^n)$, laminar and turbulent regions required different values of n, 1/3 and 1/2, respectively. Moreover, the analogy became questionable where secondary flows occur, such as blade regions affected by the passage vortex.

2. Computational model

The vane profile, which is depicted in Fig. 1-top, is typical of a first, high-pressure turbine vane of a modern heavy-duty gas turbine: the pitch-to-chord ratio and the aspect ratio are s/C = 1.04 and H/C = 0.69, respectively. The flow turning angle at design point is 73.5°. The cascade was simulated at exit Mach number of Ma_{2is} = 0.2 and inlet turbulence intensity of Tu_1 = 1.6% (Λ_x = 11.8 mm), corresponding to the free admission level, and Tu_1 = 13% (Λ_x = 14.9 mm). The leading edge is equipped with four staggered rows of cylindrical holes (Fig. 1-bottom) located at s/C equal to -0.048 (row#1), -0.017 (row#2), 0.018 (row#3), and 0.059 (row#4). Each row is composed of 16 cooling holes, whose diameter is D= 1.0 mm. Within each row, the hole-to-hole pitch is 5.9D and the hole length is 2.9D. Holes are spread over 90% of the vane height and angled at 45° to the surface. The 3D numerical domain is shown in Fig. 2: one vane passage was represented with periodicity conditions set in the tangential direction in order to simulate the linear cascade arrangement of the wind tunnel available at the "Energy Systems and Turbomachinery" laboratory. The coolant plenum, 64 cooling channels of showerhead type and the vane passage were modeled across the entire span. The inlet of the passage was located at X/C_{ax} = -1.6, i.e. where approaching main flow boundary layer, turbulence intensity and length scale were available from experiments. The outlet was located 1 C_{ax} downstream of the vane trailing edge. The boundary conditions prescribed inlet total pressure profile for the mainstream (Fig. 3) and constant static pressure at the outlet (96000 Pa), in order to ensure Ma_{2is} of 0.2. The coolant flow entering one side of the plenum was simulated in terms of inlet mass flow rate. Coolant turbulence intensity and length scale were computed from correlations of fully-developed pipe flow. BR values of 2.0, 3.0 and 4.0 were taken into account, with the medium BR of 3.0 ensuring the best trade-off between cooling air consumption and cooling efficiency. Attention was drawn to adiabatic simulations.

Even though the schematic of the computational domain is not new [24], here special care has been taken on grid generation in the showerhead region. A block, unstructured approach was used to maximize grid quality and density in the region from s/C = -0.11 on the suction side to s/C = 0.26 on the pressure side (Fig. 4). Three levels of mesh refinement were achieved by doubling and tripling the number of cells in the block surrounding the leading edge (Table 1). With the aim of fully resolving the viscous sublayers, the first grid point was located at progressively decreasing wall distance: the average y+ on the leading edge surface within -0.11< s/C <0.26 roughly halved when comparing

coarse and fine grids. Outside the leading edge block, the mesh was simply extruded in the spanwise direction to obtain the 3D vane passage. Grid generation was accomplished with Pointwise, by Pointwise, Inc.

The software Fluent v.18, by ANSYS Inc., was used to carry out the steady state simulations. The 3D Navier-Stokes equations were solved for compressible flow assuming the ideal gas law for the equation of state. The incompressible assumption could have been valid for the low speed mainstream but not for the cooling jets exiting the showerhead hole at velocity magnitude approaching the threshold value of $Ma \sim 0.3$, at the highest BR of 4.0. The Realizable k-ε turbulence model with enhanced wall treatment was used as turbulence closure, in view of more accurate predictions of laterally averaged η_{av} in the leading edge, as compared to the alternative SST k-ω turbulence model [24]. The numerical method was second order accurate in space. The residuals were about 10^{-10} for the energy equation and kept under 10^{-7} for all the other parameters. At convergence, the area weighted average η on the leading edge and along the stagnation line changed no more than 0.0005% for at least 200 iterations.

Grid independence was checked by testing the grids of Table 1. Distributions of η_{av} along the outer surface of the leading edge were computed at $BR = 3.0$, by imposing a small temperature difference between the coolant (T_c = 323 K) and the mainstream (T_∞ = 298 K). As shown in Fig. 5, there were no significant changes in η_{av} profiles between the medium and fine mesh since η_{av} deviated by less than $\varepsilon = 1.2\%$. Subsequently, the 24 million cells grid was used to run all the simulations reported in this paper.

With the mainstream flow assumed to be air at ambient temperature, the prescribed DR of 0.97 and 1.53 was achieved by injecting coolant as air at different temperature from the mainstream or as isothermal foreign gas (Table 2). Thus, for a given BR, each simulation set included four cases. For the heat transfer process (cases a, c), the well-known definition of η, at low speed, was used:

$$\eta = \frac{T_{aw} - T_\infty}{T_c - T_\infty} \qquad (6)$$

In case of mass transfer process (cases b, d), the quantity analogous to the adiabatic wall temperature T_{aw} is the mass fraction concentration (C) of oxygen inside the film ($C_{O2,fg}$), at an impermeable wall. Since N_2 and CO_2 are injected as foreign gas ($C_{O2,c} = 0$), it follows that:

$$\eta \approx \frac{C_{O_2,fg} - C_{O_2,\infty}}{C_{O_2,c} - C_{O_2,\infty}} = 1 - \frac{C_{O_2,fg}}{C_{O_2,\infty}} \qquad (7)$$

where $C_{O2,\infty}$ is a constant value (0.231).

Equation 6 is analogous to eq. 7 if the dimensionless parameters of film cooling are the same in the two cases (*a* vs. *b*, *c* vs. *d*). Moreover, both molecular Lewis number (Le) and turbulent Lewis number (Le_t) should be unity for the analogy to hold [25]. Table 3 shows the non-dimensional transport parameters for the fluids involved in the present study: film

cooling process in presence of temperature gradients is governed by the Prandlt number *Pr* whereas the Schimdt number *Sc* accounts for the mass transport process. Density (ρ) was determined from the ideal gas equation of state; dynamic viscosity (μ), thermal conductivity (k) and specific heat (c_p) were calculated from published correlations at ambient pressure [26] and verified against those computed by the CFD modeling at the inlet of the vane passage and the plenum. Values of binary diffusion coefficient D were taken from [27]: at low density, they increase with temperature. No coolant Lewis number exceeded unity by more than 10%. Instead, both Pr_t and Sc_t are characteristic features of the turbulent flow, so no universal value could be established a priori but eventually determined as simulation output.

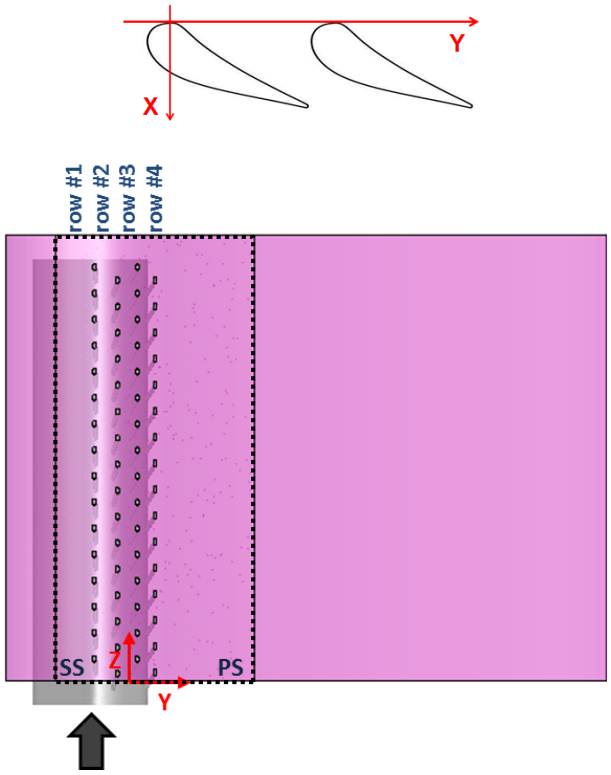

Fig. 1. Cascade model (top) and showerhead cooling scheme (bottom) [24].

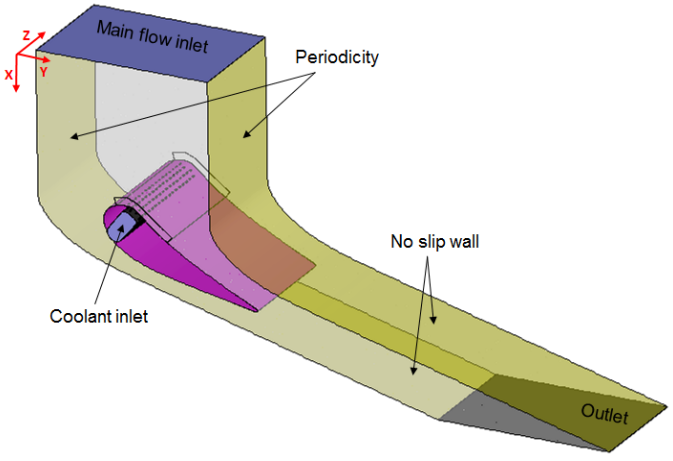

Fig. 2. Schematic of the 3D computational domain (from [24]).

Grid refinement	Coarse	Medium	Fine
Polyhedra (million)	18.48	24.36	29.52
Million cells in the LE block	5.31	11.19	16.34
LE averaged y+ (*BR* = 3.0)	3.02	1.71	1.36

Table 1. Grid refinement

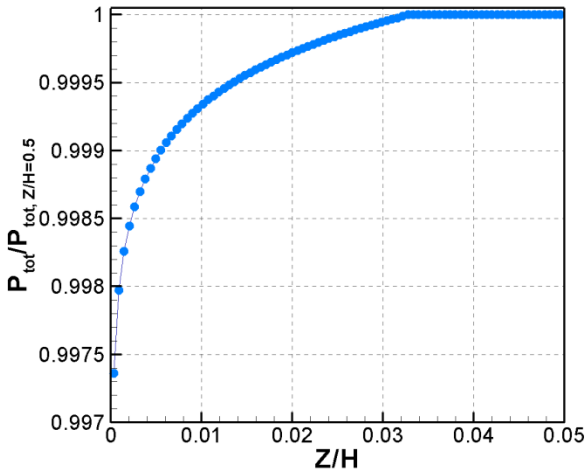

Fig. 3. Inlet total pressure profile at X/c_{ax} = -1.6.

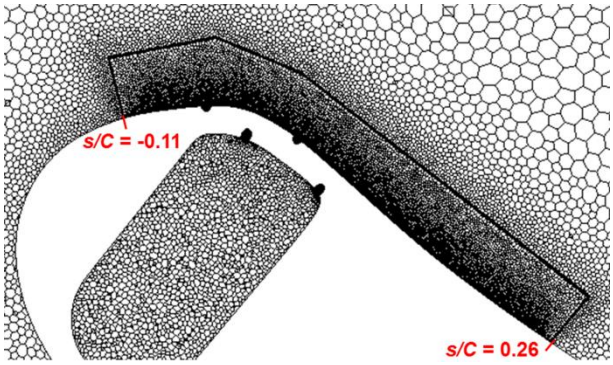

Fig. 4. Midspan view of the mesh in the leading edge region

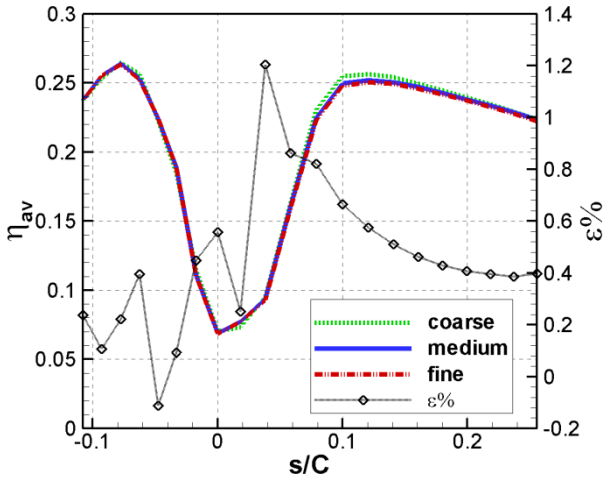

Fig. 5. Grid convergence test at *BR* = 3.0: ε is the percentage difference in η_{av} between medium and fine grid.

	***DR* = 0.97**		***DR* = 1.53**	
	Heat transfer	Mass transfer	Heat transfer	Mass transfer
Case number	**a)**	**b)**	**c)**	**d)**
Coolant flow	air	N_2	air	CO_2
Coolant temperature (T_c)	323 K	298.5 K	203 K	298.5 K
Mainstream flow	air			
Mainstream Temperature (T_∞)	298.5 K			

Table 2. Coolant and mainstream conditions for each simulation set at given *BR*.

	$Pr = \mu c_p / k$	$Sc = \mu / \rho D$	$Le = Sc / Pr$
Mainstream air (298.5 K)	0.71	0.77	1.08
Coolant air (203 K; 323 K)	0.71; 0.70	0.74; 0.77	1.04; 1.10
N_2 (298.5 K)	0.71	0.76	1.07
CO_2 (298.5 K)	0.77	0.76	0.99

Table 3. Non-dimensional heat/mass transfer parameters.

In ANSYS Fluent, turbulent heat transport is modeled using the concept of Reynolds' analogy to turbulent momentum transfer [28]. In the energy equation, the term describing conduction includes the effective thermal conductivity k_{eff} given by:

$$k_{eff} = k + k_t = k + \frac{c_p \mu_t}{Pr_t} \qquad (8)$$

where the turbulent Prandtl number has been set at Pr_t = 0.7. The turbulent viscosity μ_t is calculated by means of the Realizable k-ε turbulence model, according with:

$$\mu_t = \rho C_\mu \frac{k^2}{\varepsilon}, \text{ where } C_\mu = 0.09 \qquad (9)$$

Similarly, the effective viscosity μ_{eff} is defined as a sum of laminar and turbulent viscosity:

$$\mu_{eff} = \mu + \mu_t \qquad (10)$$

Dilute approximation (also called Fick's law) was used to model mass diffusion due to concentration gradients. The effective mass diffusion coefficient D_{eff}, for the species *i* in the mixture, is defined as:

$$D_{eff} = D + D_t = D + \frac{\mu_t}{\rho Sc_t} \qquad (11)$$

where the turbulent Schmidt number has been set at Sc_t = 0.7.

3. Results and discussion

For each injection condition, four simulation scenarios are presented to investigate the influence of *DR* on the leading edge film cooling effectiveness, by using thermal and mass transfer approaches. Results for *BR* = 3.0 are presented first at low mainstream turbulence, contextually with validation against measurements. In the following, results from higher

and lower *BR* are also reported for a complete discussion of the heat-mass transfer analogy, by varying the injection rate. Finally, the role played by high mainstream turbulence in determining η was also assessed, for the reference *BR* value of 3.0.

3.1. Showerhead film cooling at *BR* = 3.0

Figure 6 compares the adiabatic effectiveness contours from PSP technique at *DR*= 0.97 and 1.53 with results from simulations using the heat and mass transfer methods. The region of interest for this study was within -0.11 < *s/C* < 0.26, i.e. where the mesh near the wall is properly sized, and 0 < *Z/H* < 0.7, where PSP data were available. Please note that the coolant is supplied from the hub side (*Z/H* = 0) and jets are blowing towards positive values of *z*. Both measurements and simulations showed that spanwise uniformity cannot be established in the contours of η, whatever the *DR*: in particular, the region of the vane near the hub (*Z/H* < 0.15) is poorly cooled since the coolant tends to accumulate towards the tip. Jets exit rows 2-4 in positive y-direction whereas jets from row#1 flow in negative y-direction, thus contributing to suction side film cooling. On the pressure side, the oblique travelling of the coolant led to high effectiveness downstream of row#2, at *z/H* > 0.2; merging of the coolant jets just downstream of row#4 caused the highest levels of η at about 0.6. On the suction side, jets from row#1 separate and reattach downstream causing an almost periodic pattern of η at *s/C* < -0.07 and *Z/H* > 0.3. As a general comment, the increase in *DR* yielded superior performance of the showerhead cooling scheme: jet velocity at the outlet of the coolant channels is reduced by a factor of 1.5 so jet penetration into the mainstream is weakened and protection on the surface is enhanced.

Differences between simulations and experimental data but, above all, between the simulation approaches are evident from Fig. 6 when comparing the results at low (top) and high (bottom) *DR*. For quantitative assessment of results, η values were laterally averaged over the span section between *Z/H* = 0 and 0.7, even though periodicity does not exist (Fig. 7). Focusing on the former aspect, despite weak overprediction of η levels, modelling correctly predicted the rising trend of η in the showerhead region (within -0.048< *s/C* < 0.059), at increasing *s/C*, whatever the *DR*. This is due to the coolant outflow from rows 2-4 building up a film layer. On the pressure side, measured and computed slope of the decreasing η_{av} function at *s/C* > 0.15 are in very good agreement, with slight underestimation of η_{av} levels in case of low *DR*. In that region, turbulent dispersion of the coolant jets has a detrimental effect on film coverage. The limitations of the steady modelling arose just downstream of row#4 (*s/C* =0.06), where pressure side jets merge due to the spanwise motion: overestimation of η_{av} was more severe in case of high *DR*, due to the reduced jet momentum. Another crucial region of the vane is defined as *s/C* < -0.07: η underprediction occurred downstream of row#1 due to excessive jet separation. The application of the scale resolving simulation techniques, such as detached eddy simulation, would

have improved the accuracy of η predictions, especially on the suction side [24]. However, it was felt unsuitable because of excessive computational effort, given the numerous simulations (16) reported in the current study.

After successful validation of the modelling procedure, which was found to match the η_{av} trends shown in the experimental data for most of the selected range of *s/C*, attention was given to the fact that simulations using heat and mass transfer approaches yielded different results. At low *DR*, the most significant discrepancy when comparing cases *a* vs. *b* occurred immediately downstream of row#4, where nitrogen jet produced η_{av} values up 15% higher as compared to the correspondent hot jet. Furthermore nitrogen jet trajectories on the pressure side have lower lateral (streamwise) deflection, being more similar to those displayed by the PSP technique. This was despite the fact that film cooling parameters at matched *BR* condition are practically the same for cases *a* and *b*, as shown in Table 4.

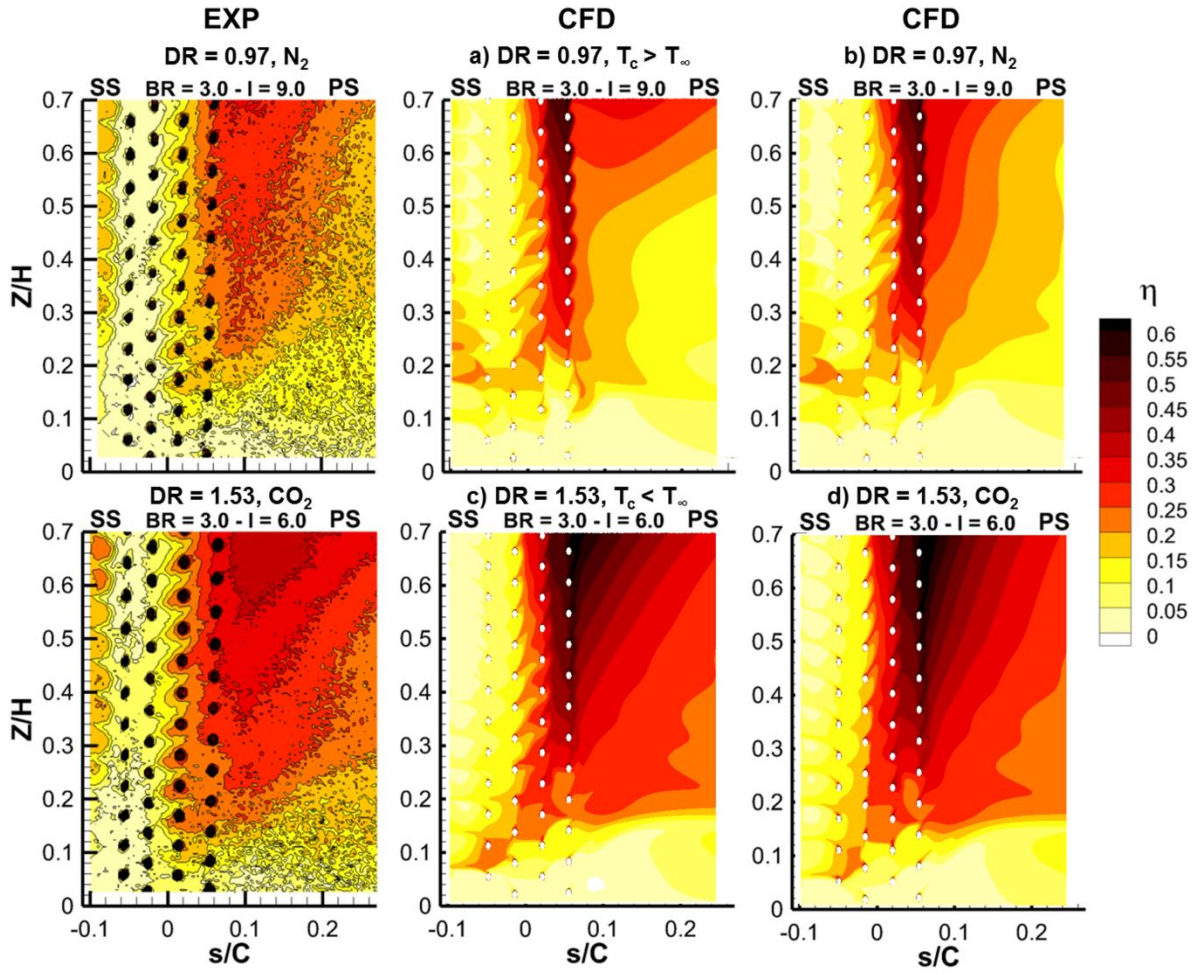

Fig. 6. Contours of adiabatic effectiveness η from PSP measurements (left), heat (middle) and mass (right) transfer simulation method for a,b) DR = 0.97, BR = 3, I = 9 and c,d) DR = 1.53, BR = 3, I = 6.

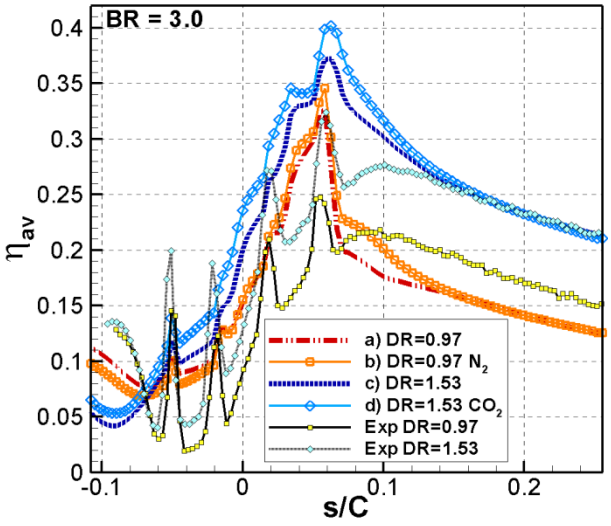

Fig. 7. Profiles of laterally averaged adiabatic effectiveness η_{av} from PSP measurements (Exp), heat and mass transfer simulation method for a,b) DR = 0.97, BR = 3, I = 9 and c,d) DR = 1.53, BR = 3, I = 6.

BR = 3.0	DR	**BR**	VR	I	$c_{p,c}/c_{p,\infty}$	ACR
a) DR = 0.97	0.97	**3.0**	3.09	9.28	1.00	3.00
b) DR = 0.97 N_2	0.97	**3.0**	3.09	9.27	1.03	3.08
c) DR = 1.53	1.53	**3.0**	1.97	5.90	1.00	3.00
d) DR = 1.53 CO_2	1.53	**3.0**	1.97	5.90	0.84	2.52

Table 4. Non-dimensional film cooling parameters at matched *BR* conditions.

It should be noted that *BR* was rearranged as:

$$BR = \frac{m_c A_\infty}{m_\infty A_c} \qquad (12)$$

where A_c and A_∞ are the showerhead channel area and the inlet sectional area of the cascade, respectively. Accordingly, "overall" definition of *VR* and *I* were used:

$$VR = \frac{BR}{DR} \qquad (13)$$

$$I = \frac{BR^2}{DR} \qquad (14)$$

At high *DR*, the carbon dioxide jets of Fig. 6d produced a flow pattern quite similar to that of the cold air jets in Fig. 6c, at least from a qualitative point of view. However, overestimation of η_{av} is evident on the pressure side within $s/C <$ 0.16 and over the whole showerhead region. The degree of overestimation is within 10% in the former case and in the range between 13% and 20% at $-0.048 < s/C < 0$. Moreover, the footprint of the carbon dioxide jets exiting row#1 can be clearly seen, differently than in case *c*, thus providing greater airfoil protection on the suction side: η_{av} is 24% higher

at *s/C* = -0.095 for case *d* when compared to case *c*. The actual *ACR* is of particular importance when using CO_2 coolant: even at matched *BR* conditions, *ACR* is only 2.52 as shown in Table 4, due to the significant difference in c_p value from that of air.

3.2. Showerhead film cooling at *BR* = 4.0

The predicted adiabatic effectiveness performance for the leading edge region at *BR* = 4.0 is presented in Fig. 8. The average exit velocity of the showerhead jets is approximately 30% higher as compared to *BR* = 3.0. All the reported simulation scenarios have in common a dramatic accumulation of the coolant toward the tip in the jet exit direction, whose effect on η is particularly noteworthy on the pressure side. Accordingly, there is a very poor spanwise uniformity and effectiveness levels are quite low over the first half of the span. This is especially true at low *DR*: both Figs. 4a and 4b show a wide region where $\eta < 0.15$, extending on the pressure side (at *s/C* > 0.06, within *Z/H* < 0.5) and in between row#1 and row#2. The cooling jets from holes located close to the hub side, having the largest momentum within each row, separate from the vane surface and (partially) reattach at higher *Z/H* positions: this is why the leading edge is almost uncooled at low *Z/H* values.

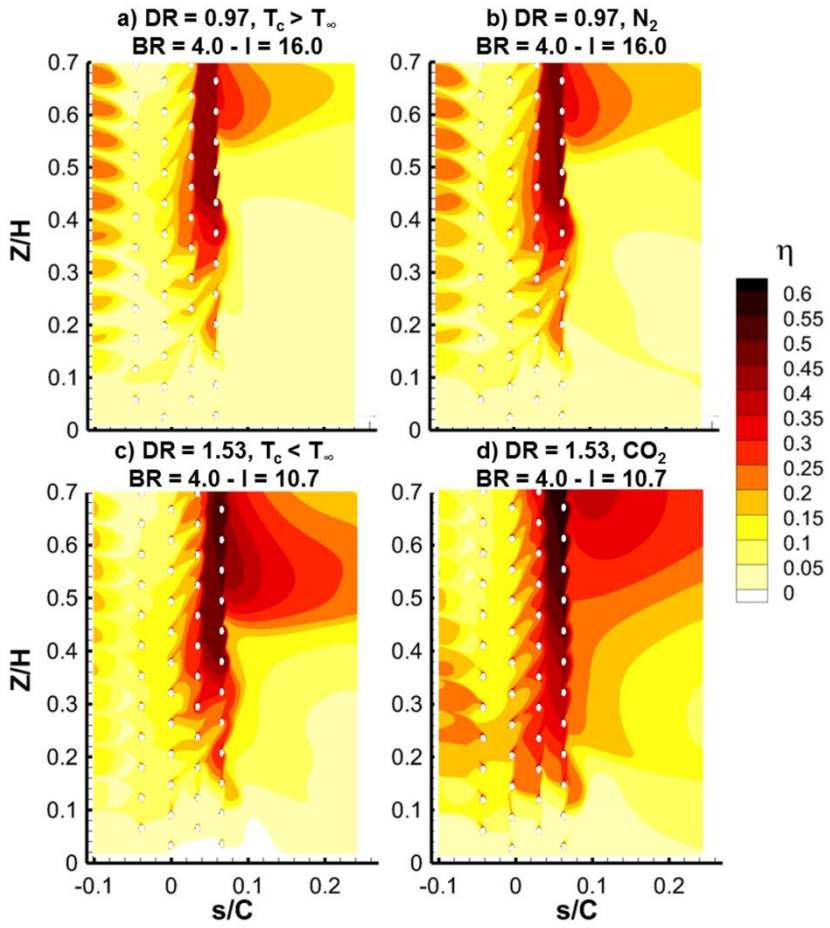

Fig. 8. Predicted contours of adiabatic effectiveness η using heat (left) and mass (right) transfer method for a,b) DR = 0.97, BR = 4, I = 16 and c,d) DR = 1.53, BR = 4, I = 10.7.

In particular, cooling jets from rows#2-4 concur to effectively cool the showerhead region between row#3 and row#4, at Z/H > 0.3, and downstream of row#4, at Z/H > 0.5. Conversely, separated cooling jets from row#1 are re-directed towards the suction side by the action of the accelerating main flow: roughly periodic pattern of η can be detected starting from Z/H of about 0.2, with increasing η levels at Z/H > 0.4. The average velocity of the showerhead jets decreases from 94 m/s to about 60 m/s when increasing the *DR* from 0.97 to 1.53: *I* decreases as well from 16.5 to 10.5 (Table 5). Hence, there still might be separation of the cooling jets due to the highest *BR*, as proved by very low η values within Z/H < 0.1, but with a minor detrimental effect on η (Figs. 8c,d). In fact, high-density jets enhanced the lateral coverage on the pressure side, downstream of row#4, and the spanwise coverage between row#2 and #4.

The point is that the simulation approach deeply affected distribution and level of η, whatever the *DR*. Similarly to the case with *BR* = 3.0, the mass transfer method gave higher η_{av} values than those from the heat transfer method, but here the difference between foreign gas and air jets, in terms of $\eta_{av,}$ is much more significant (Fig. 9). The profiles of η_{av} with nitrogen coolant (*b*) is shifted upward as compared with regular air (*a*), thus indicating lower dispersion of the film layer: overprediction in η_{av} is between 20% and 26% on the pressure side, where $\eta_{av} < 0.1$, and between 15% and 35% on the suction side. However, cases at high *DR* are the greatest threat to the validity of the heat/mass transfer analogy. At s/C > 0.1, higher η_{av} values were obtained using carbon dioxide jets, as compared to cold air jets, with a less severe declining trend in η_{av} while increasing s/C, hence the largest degree of overestimation (+28%) was observed at s/C = 0.26. On the suction side, an upward shift of the η_{av} curve can be noticed for case *d*, compared to case *c*, with a dramatic 80% difference where η_{av} reaches the minimum at s/C = -0.07. Using carbon dioxide rather than cold air improved cooling performance also in the showerhead region except in close proximity of row#4, at s/C = 0.06, where profiles *c* and *d* collapse into one point. Again, ACR is the only difference between cases *c* and *d* at matched *BR* condition (Table 5).

BR = 4.0	DR	**BR**	VR	I	$c_{p,c}/c_{p,\infty}$	ACR
a) DR = 0.97	0.97	**4.0**	4.12	16.49	1.00	4.01
b) DR = 0.97 N_2	0.97	**4.0**	4.12	16.49	1.03	4.11
c) DR = 1.53	1.53	**4.0**	2.61	10.46	1.00	4.01
d) DR = 1.53 CO_2	1.53	**4.0**	2.61	10.46	0.84	3.36

Table 5. Non-dimensional film cooling parameters at matched *BR* conditions.

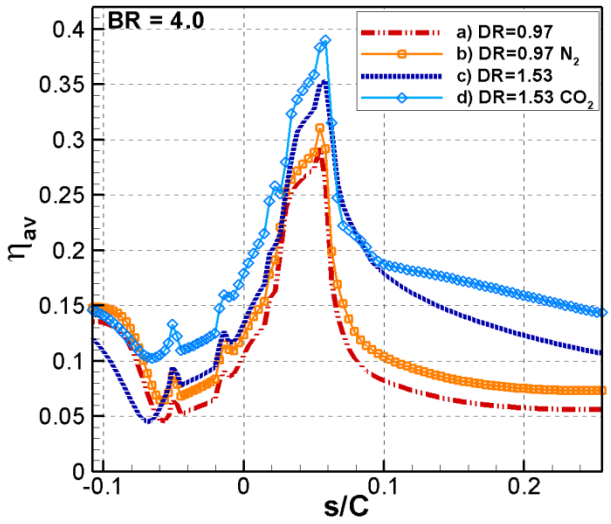

Fig. 9. Predicted profiles of laterally averaged adiabatic effectiveness η_{av} from heat and mass transfer simulation method for a,b) DR = 0.97, BR = 4, I = 16 and c,d) DR = 1.53, BR = 4, I = 10.7.

3.3. Showerhead film cooling at *BR* = 2.0

Figure 10 shows the distributions of film cooling effectiveness for the lowest *BR* value of 2.0. There is no doubt, of course, that reducing the *BR* allowed the jets to stay attached over more of the leading edge surface: *VR* is about 2 at low *DR* and slightly more than 1 at high *DR* (Table 6). The positive effect on η was especially evident on the pressure side, where rows 2-4 provided the largest film cooling coverage for the investigated range of showerhead blowing conditions, in case of low *DR* (Fig. 10a,b): merging of the coolant jets with oblique trajectory yielded the best thermal protection at *s/C* > 0.06, over most of the span. Conversely, the decrease in *BR* from 3.0 to 2.0 was less beneficial at high *DR*: the comparison between Figs. 10c,d and Figs. 6c,d highlighted the worse performance of the blowing condition of *BR* = 2.0 downstream of row#4, within the first half of the vane span.

Unlike that displayed on the pressure side, cooling performance on the suction side was found to be negatively affected by decreasing *BR*, at low *DR*: narrow traces of the jets from row#1 are clearly visible at *s/C* < -0.05 in Figs. 10a,b but interspersed with quite wide regions of extremely low effectiveness (η < 0.05). At high *DR*, the gaps between the jets from row#1 are filled by values of η between 0.1 and 0.15, as shown in Figs. 10c,d. The resulting flow pattern on the suction side is quite similar to that of Figs. 6c,d thus suggesting that the mainstream dominates the coolant jets from row#1 to produce comparable effectiveness levels, as long as their exit velocity is lower than 45 m/s. It follows that overall *VR* and *I* could appear insufficient to explain the complex mechanisms underlying the jet-mainstream interaction, either it is row-to-row or hole-to-hole.

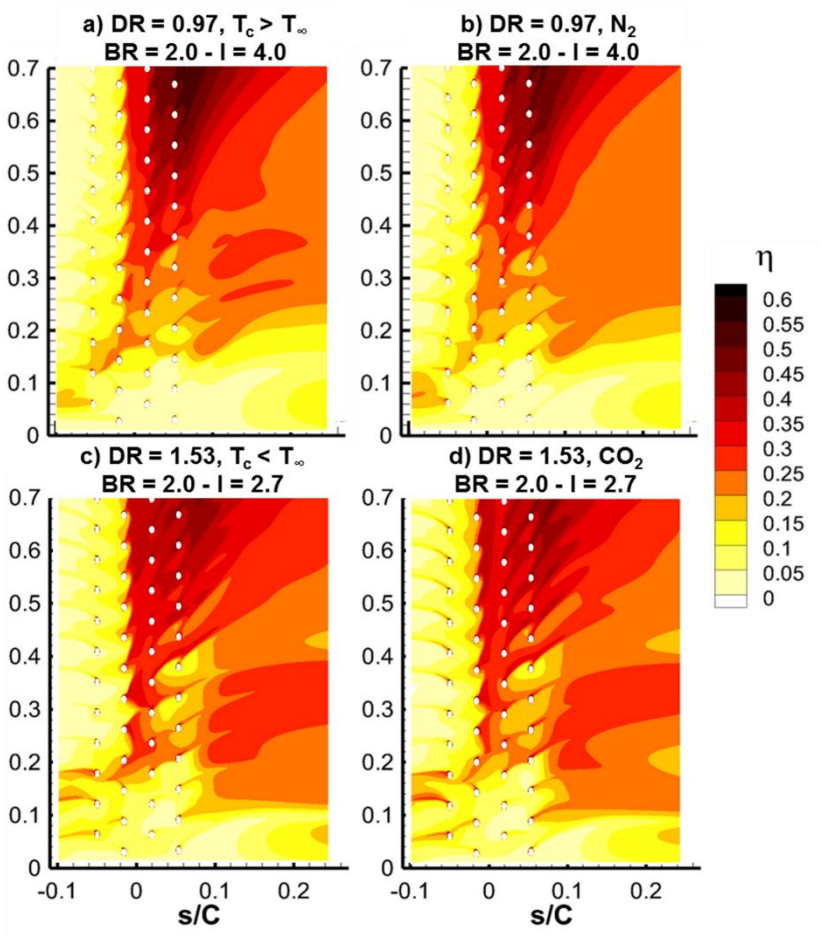

Fig. 10. Predicted contours of adiabatic effectiveness η using heat (left) and mass (right) transfer method for a,b) DR = 0.97, BR = 2, I = 4 and c,d) DR = 1.53, BR = 2, I = 2.7.

BR = 2.0	DR	**BR**	VR	I	$c_{p,c}/c_{p,\infty}$	ACR
a) DR = 0.97	0.97	**2.0**	2.06	4.12	1.00	2.00
b) DR = 0.97 N_2	0.97	**2.0**	2.06	4.12	1.03	2.06
c) DR = 1.53	1.53	**2.0**	1.31	2.61	1.00	2.00
d) DR = 1.53 CO_2	1.53	**2.0**	1.31	2.61	0.84	1.68

Table 6. Non-dimensional film cooling parameters at matched *BR* conditions.

Again, simulation results were reported in terms of η_{av} (Fig. 11). In contrast to the cases above, small deviations occurred between heat and mass transfer predictions. The percentage difference between profiles *a* and *b* and between profiles *c* and *d* is within $\varepsilon = \pm 7\%$ on the pressure side and in the showerhead region. On the suction side, at *s/C* < -0.05, foreign gas as coolant produced slightly higher η_{av} than the correspondent air case. This is especially true for the carbon dioxide jets, for which η_{av} is up to 18% higher than that of cold air. However, this percentage might be misleading, due to the extremely low levels of η_{av} in the considered region.

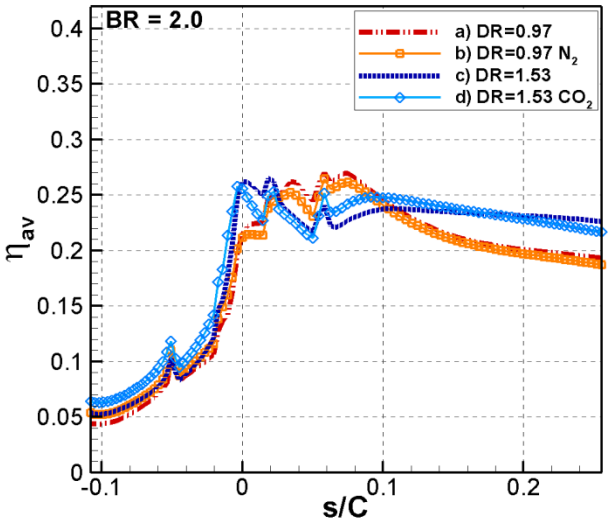

Fig. 11. Predicted profiles of laterally averaged adiabatic effectiveness η_{av} from heat and mass transfer simulation method for a,b) DR = 0.97, BR = 2, I = 4 and c,d) DR = 1.53, BR = 2, I = 2.7.

3.4. Showerhead film cooling at *BR* = 3.0 with high inlet turbulent intensity

All the four simulations scenarios were computed for the medium *BR* of 3.0, with Tu_1 = 13%. Results were presented as contour plots of η (Fig. 12) and distributions of η_{av} (Fig. 13). The relevant changes in respect of the case at low Tu_1 deal with less sensitivity to coolant jet separation on the suction side, at *s/C* < -0.05, and greater spanwise spreading of the coolant in between rows#2-4, especially at high *DR*. The high level of Tu_1 helped to dampen the differences in η_{av} due to the used approach only in case of *DR* = 1.5, when the *VR* is about 2. Conversely, at *DR* ~ 1 and *VR* of about 3, there are still remarkable differences in the coolant trajectory on the pressure side between cases *a* and *b*, with nitrogen jets providing enhanced cooling performance. Curve *b* shows higher η_{av} than curve *a* at *s/C* > 0: the percentage difference is the highest (ε = +22%) at *s/C* = 0.09 and goes down to ε = 1.5% at *s/C* = 0.26.

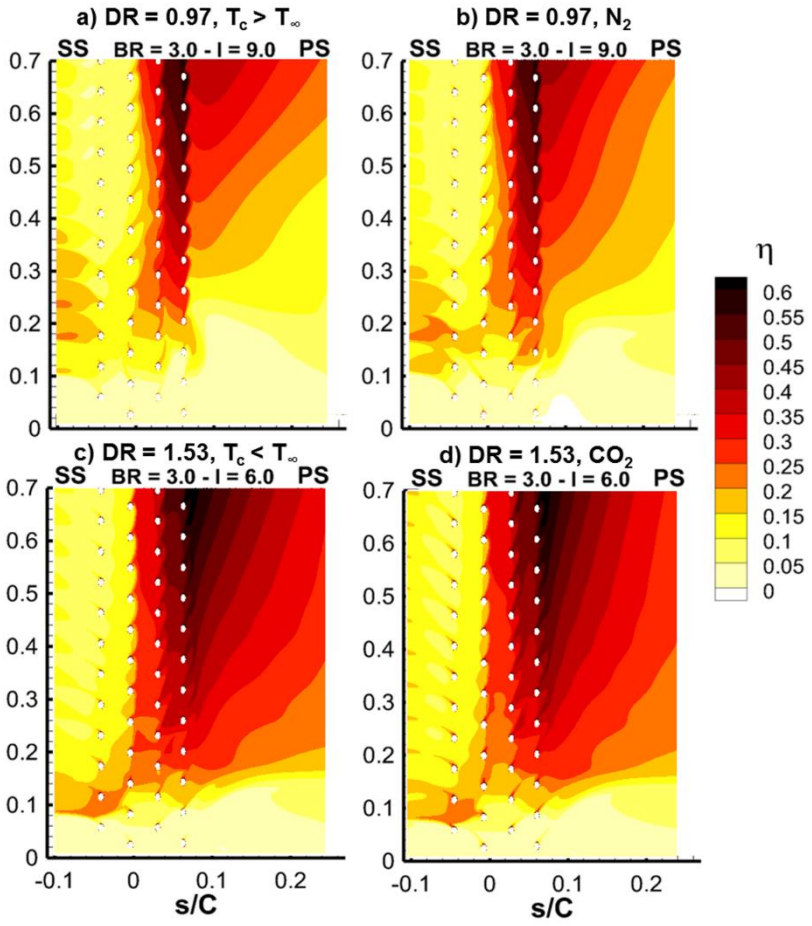

Fig. 12. Predicted contours of adiabatic effectiveness η using heat (left) and mass (right) transfer method for a,b) DR = 0.97, BR = 3, I = 9 and c,d) DR = 1.53, BR = 3, I = 6 at Tu_1 = 13%.

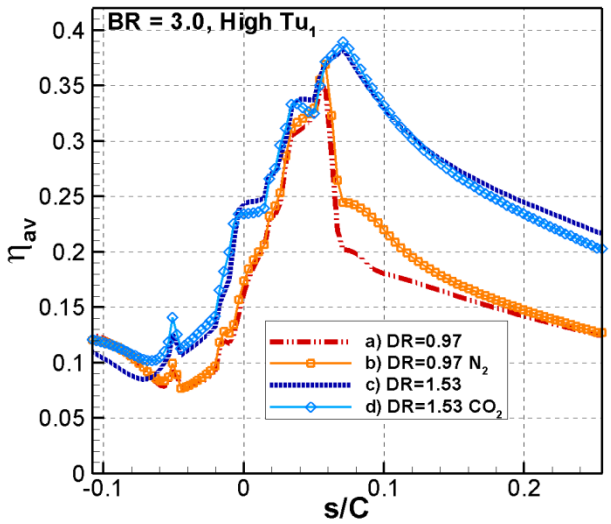

Fig. 13. Predicted profiles of laterally averaged adiabatic effectiveness η_{av} from heat and mass transfer simulation method for a,b) DR = 0.97, BR = 3, I = 9 and c,d) DR = 1.53, BR = 3, I = 6 at Tu_1 = 13%.

3.5. On the validity of the heat and mass transfer analogy

In order to achieve a comprehensive evaluation of the impact of the simulation approach on film cooling predictions, values of area-averaged adiabatic effectiveness were presented in Table 7, for all 16 cases. The percentage difference ε between the results provided by the two methods, i.e. using either heat or mass transfer process, was also computed. ε can be regarded as negligible at the lowest *BR* value of 2.0, whatever the *DR*. Conversely, values of ε higher than 17% were found at *BR* = 4.0, thus confirming poor applicability of the heat and mass transfer analogy for the highest blowing condition. For the medium *BR* of 3.0, a distinction should be made between high and low *DR*. In the former case, ε is somewhat acceptable at low Tu_1 and practically zero at high Tu_1 whereas in the latter case, area averaged η is over predicted by more than 10% with nitrogen coolant compared to air, whatever the inlet turbulence intensity.

Potential sources of the reported discrepancy ε were further investigated. Since Table 3 has already shown that molecular *Le* is close to unity, attention was drawn to Le_t. The effective *Pr* available from the simulation cases *a* and *c* was placed side by side to effective *Sc* from cases *b* and *d*, for the reference *BR* value of 3.0 (Fig. 14). Please note that every contour plot has its own legend box, to highlight spatial details over the leading edge region. Distributions of Pr_{eff} and Sc_{eff} differ from each other quite substantially at *DR* ~ 1 whereas they look quite similar at *DR* ~1.5, at least on the pressure side. The most relevant information from Fig. 14 is the computed range of Pr_{eff} and Sc_{eff}. The former is between 0.70 and 0.77 for air as coolant whereas the latter varies from 0.52 to 0.57 or from 0.40 to 0.53 depending on the foreign gas (nitrogen or carbon dioxide, respectively). Since the reported ranges of Pr_{eff} and Sc_{eff} remain valid for *BR* values of 4.0 and 2.0, it can be deduced that Le_t does not make the difference that it should between low and high applicability of the heat and mass transfer analogy. Accordingly, the focus has shifted towards the coolant jet characteristics in terms of Reynolds number Re_c. As far as the approaching mainstream is concerned, the undisturbed flow is laminar at the leading edge of the vane [29]. Figure 15 shows the average Re_c for the entire showerhead: density, velocity and dynamic viscosity were available from the simulations as mass-weighted-average at the cooling hole exit. Obviously, Re_c increases with *BR*. For cases *c* and *d*, it results from a combination of increased coolant density and decreased jet exit velocity; among the four cases, Re_c is the highest when cold air is injected as coolant (*c*), due to the lowest viscosity.

	a) DR=0.97	b) DR=0.97 N_2	**ε (%)**	c) DR=1.53	d) DR=1.53 CO_2	**ε (%)**
BR = 2.0	0.182	0.181	**-0.6**	0.193	0.201	**4.2**
BR = 3.0	0.139	0.155	**10.9**	0.216	0.230	**6.2**
BR = 4.0	0.098	0.117	**17.6**	0.149	0.180	**18.8**
BR = 3.0 High Tu_1	0.152	0.172	**12.4**	0.236	0.236	**-0.3**

Table 7. Area-averaged η from heat (a,c) and mass (b,d) transfer simulation method, for different blowing conditions.

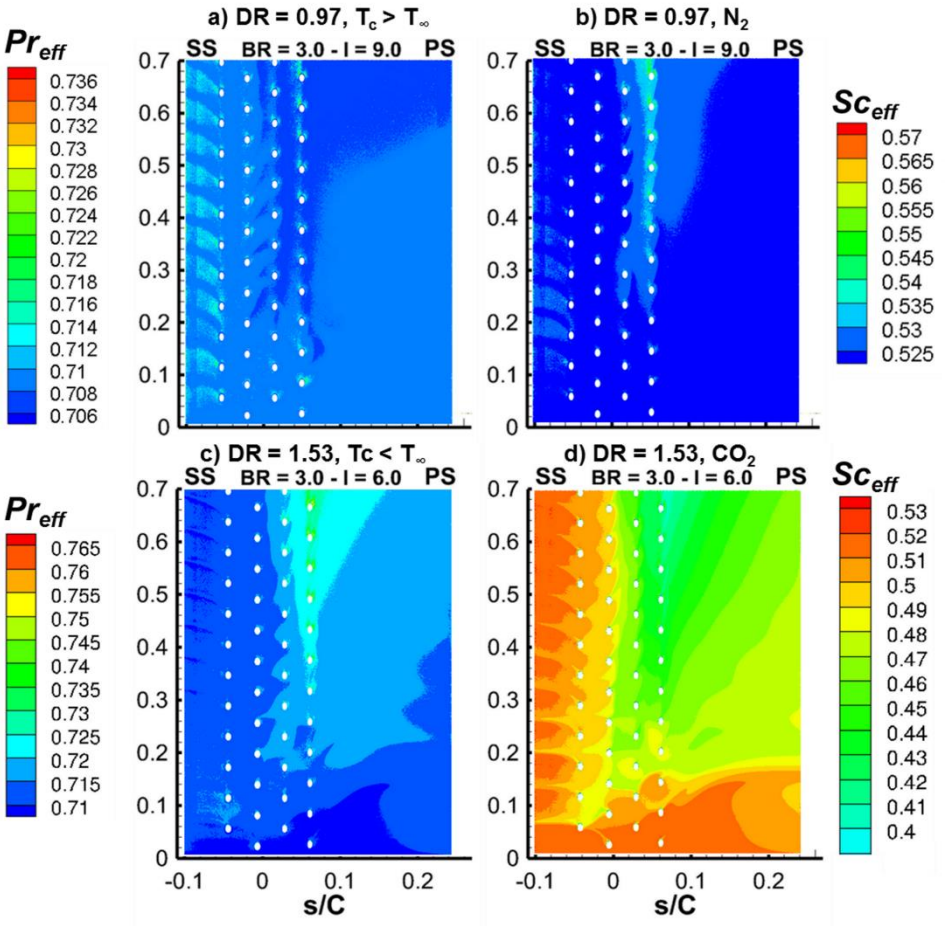

Fig. 14. Predicted contours of effective *Pr* (left) and *Sc* (right) for a,b) DR = 0.97, BR = 3, I = 9 and c,d) DR = 1.53, BR = 3, I = 6.

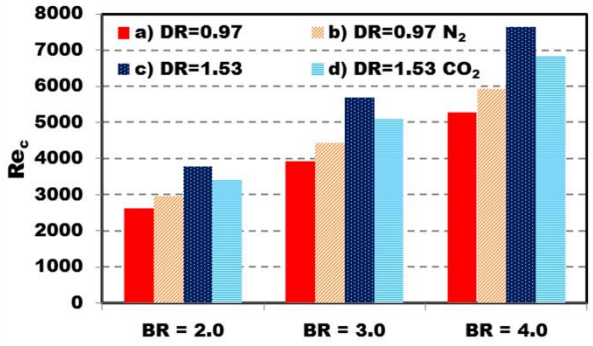

Fig. 15. Average coolant channel Reynolds number Re_c from heat (a,c) and mass (b,d) transfer simulation method, for different blowing conditions (Tu_1 = 1.6%).

At low inlet turbulence intensity, the heat and mass transfer analogy has reasonable applicability for leading edge film cooling provided that Re_c < 4000, i.e. for laminar and transitional showerhead jets [30]. In other words, cooling performance of turbulent jets, for which Re_c > 4000, depends on the used method. With high mainstream turbulence, greater dispersion of the coolant might contribute to evening out differences between the heat and mass transfer approach, provided that *VR* is sufficiently low, so that separated jets are dispersed back to the wall [16].

4. Conclusions

Steady-state numerical simulations of showerhead film cooling were performed to verify the applicability of the heat/mass transfer analogy when predicting the thermal coverage on the leading edge region, at three different blowing ratios (*BR* = 2.0, 3.0 and 4.0). Operating conditions were taken from the experimental testing at low speed passage flow (Ma_{2is} = 0.2), in which the PSP technique was used to measure the adiabatic effectiveness for two different density ratios (DR ~ 1 and 1.5), at matched *BR* conditions. The problem has been transferred from the "heat" domain to the "mass" domain by injecting coolant as air at different temperature from the mainstream or as isothermal foreign gas (i.e. nitrogen or carbon dioxide).

A good correspondence between the two simulation methods was found at the lowest *BR* of 2.0, both in terms of coolant distribution and area-averaged η. Conversely, 18% overestimation on area-averaged η resulted from applying the mass transfer method, at the highest *BR* of 4.0. Higher levels of η were predicted also at the medium *BR* of 3.0, when injecting nitrogen instead of regular air: the degree of overestimation was as high as 12%, despite perfect matching of the most relevant non-dimensional film cooling parameters, including the advective capacity ratio. The heat and mass transfer analogy was valid at the *BR* of 3.0 just in case of high *DR* and high mainstream turbulence: a reduced jet exit velocity combined with enhanced coolant dispersion led to very similar η distribution and levels, whether the coolant is cold air or carbon dioxide.

Another point worth noting is that Le_t did not make the difference between low and high applicability of the heat and mass transfer analogy. Within the present simulation framework, at low mainstream turbulence, the authors' view on the matter is that "heat" and "mass" domains are interchangeable provided that the flow through the showerhead holes is laminar and transitional, i.e. $Re_c < 4000$. Further investigation is certainly needed to assess the influence of Re_c/Re_∞ on leading edge film cooling performance, being aware that laminar cooling flow is not representative of engine conditions.

Nomenclature

A	cross-sectional area, m^2
ACR	advective capacity ratio, ACR = $\rho_c U_c c_{P,c}/\rho_\infty U_\infty c_{P,\infty}$
BR	blowing ratio, $BR = \rho_c U_c/\rho_\infty U_\infty$
C	vane chord, m
	mass fraction concentration
c_P	specific heat at constant pressure, J/(kg K)
C_μ	turbulence model constant

CFD	computational fluid dynamics
D	hole diameter, m
Ɗ	binary diffusion coefficient, m^2/s
DR	density ratio, $DR = \rho_c/\rho_\infty$
H	vane height, m
I	momentum flux ratio, $I = \rho_c U_c^2/\rho_\infty U_\infty^2$
IR	infrared thermography
k	thermal conductivity, W/(m K)
	turbulent kinetic energy, m^2/s^2
Le	Lewis number, $Le = Sc/Pr$
m	mass flow rate, kg/s
Ma	Mach number
Nu	Nusselt number
Pr	Prandtl number, $Pr = \mu c_p/k$
PSP	pressure sensitive paint
Re_c	Reynolds number referred to cooling holes, $Re_c = \rho_c U_c D/\mu$
Re_x	Reynolds number referred to blade [22], $Re_x = \rho_\infty U_x C/\mu$
s	vane pitch, m
	curvilinear coordinate, m
Sc	Schmidt number, $Sc = \mu/\rho Ɗ$
Sh	Sherwood number
SST	shear-stress transport
T	temperature, K
Tu	turbulence intensity (%)
U	velocity magnitude, m/s
VR	velocity ratio, $VR = U_c/U_\infty$
X	X-coordinate, axial direction, m
y^+	Dimensionless wall distance
Y	Y-coordinate, tangential direction, m
Z	Z-coordinate, spanwise direction, m

ε	dissipation rate, 1/s
	percentange difference between a and b, $\varepsilon = (b-a)/(b+a)/2*100$
η	adiabatic effectiveness, $\eta = (T_{aw} - T_\infty)/(T_c - T_\infty)$
Λ_x	streamwise integral length scale (m)
μ	dynamic viscosity, kg/(m s)
ρ	density, kg/m^3
ω	specific dissipation rate, 1/s

Subscripts

1	inlet
2	exit
av	average
aw	adiabatic wall
ax	axial direction
c	cooling flow
eff	effective
fg	foreign gas
is	isentropic condition
P	pressure
t	turbulent
x	main stream direction
∞	free stream

Superscripts

n	exponent

Acknowledgments

The authors acknowledge CINECA and Regione Lombardia award under the LISA initiative 2016-2018, for the availability of high performance computing resources and support.

References

[1] Cunha, F. J., 2006, “Heat Transfer Analysis”, chapter 4.4, The gas turbine handbook, NETL**.**

[2] Goldstein, R. J., Jin, P., & Olson, R. L. (1999). Film cooling effectiveness and mass/heat transfer coefficient downstream of one row of discrete holes. Journal of turbomachinery, 121(2), 225-232.

[3] Goldstein, R. J., & Jin, P. (2000, May). Film cooling downstream of a row of discrete holes with compound angle. In ASME Turbo Expo 2000: Power for Land, Sea, and Air (pp. V003T01A054-V003T01A054). American Society of Mechanical Engineers.

[4] Johnson, B., Tian, W., Zhang, K., & Hu, H. (2014). An experimental study of density ratio effects on the film cooling injection from discrete holes by using PIV and PSP techniques. *International Journal of Heat and Mass Transfer*, *76*, 337-349.

[5] Abdeh, H., Miranda, M., Rouina, S., & Barigozzi, G. (2017). Development of PSP Technique for Vane Film Cooling Investigations. Energy Procedia, 126, 802-809.

[6] Jones, T. V. (1999). Theory for the use of foreign gas in simulating film cooling. International Journal of Heat and Fluid Flow, 20(3), 349-354.

[7] Han, J. C., & Rallabandi, A. (2010). Turbine blade film cooling using PSP technique. Frontiers in Heat and Mass Transfer (FHMT), 1(1).

[8] Ahn, J., Schobeiri, M. T., Han, J. C., & Moon, H. K. (2006). Film cooling effectiveness on the leading edge region of a rotating turbine blade with two rows of film cooling holes using pressure sensitive paint. Journal of heat transfer, *128*(9), 879-888.

[9] Li, S. J., Yang, S. F., & Han, J. C. (2014). Effect of coolant density on leading edge showerhead film cooling using the pressure sensitive paint measurement technique. Journal of Turbomachinery, 136(5), 051011.

[10] Zhang, M., Wang, N., Chen, A. F., & Han, J. C. (2017, June). Influence of Turbine Blade Leading Edge Profile on Film Cooling with Shaped Holes. In ASME Turbo Expo 2017: Turbomachinery Technical Conference and Exposition (pp. V05CT19A010-V05CT19A010). American Society of Mechanical Engineers.

[11] Johnson, B., & Hu, H. (2016). Measurement uncertainty analysis in determining adiabatic film cooling effectiveness by using pressure sensitive paint technique. Journal of Turbomachinery, 138(12), 121004.

[12] Natsui, G., Little, Z., Kapat, J. S., Dees, J. E., & Laskowski, G. (2016). A detailed uncertainty analysis of adiabatic film cooling effectiveness measurements using pressure-sensitive paint. *Journal of Turbomachinery*, *138*(8), 081007.

[13] Wiese, C. J., Rutledge, J. L., & Polanka, M. D. (2018). Experimental Evaluation of Thermal and Mass Transfer Techniques to Measure Adiabatic Effectiveness With Various Coolant to Freestream Property Ratios. Journal of Turbomachinery, 140(2), 021001.

[14] Barigozzi, G., Casarsa, L., Pagnacco, F, Samaneh, R. (2018). Experimental Investigation of the interaction between showerhead coolant jets and main flow, submitted to the International Journal of Heat and Fluid Flow, under review.

[15] Ethridge, M. I., Cutbirth, J. M., & Bogard, D. G. (2000, May). Scaling of performance for varying density ratio coolants on an airfoil with strong curvature and pressure gradient effects. In ASME Turbo Expo 2000: Power for Land, Sea, and Air (pp. V003T01A047-V003T01A047).

[16] Cutbirth, J. M., & Bogard, D. G. (2003, January). Effects of coolant density ratio on film cooling performance on a vane. In ASME Turbo Expo 2003, collocated with the 2003 International Joint Power Generation Conference (pp. 385-394).

[17] Rutledge, J. L., & Polanka, M. D. (2014). Computational Fluid Dynamics Evaluations of Unconventional Film Cooling Scaling Parameters on a Simulated Turbine Blade Leading Edge. Journal of Turbomachinery, 136(10), 101006.

[18] Beirnaert-Chartrel, G., & Bogard, D. G. (2012, June). CFD Predictions of Heat Transfer Coefficient Augmentation on a Simulated Film Cooled Turbine Blade Leading Edge. In ASME Turbo Expo 2012: Turbine Technical Conference and Exposition (pp. 1725-1735).

[19] Eckert, E. R. G., Sakamoto, H., & Simon, T. W. (2001). The heat/mass transfer analogy factor, Nu/Sh, for boundary layers on turbine blade profiles. International Journal of Heat and Mass Transfer, 44(6), 1223-1233.

[20] Kulkarni, K. S., Madanan, U., Mittal, R., & Goldstein, R. J. (2017). Experimental validation of heat/mass transfer analogy for two-dimensional laminar and turbulent boundary layers. International Journal of Heat and Mass Transfer, 113, 84-95.

[21] Mittal, R., Madanan, U., & Goldstein, R. J. (2017). The heat/mass transfer analogy for a backward facing step. International Journal of Heat and Mass Transfer, 113, 411-422.

[22] Han, S., & Goldstein, R. J. (2008). The heat/mass transfer analogy for a simulated turbine blade. International Journal of Heat and Mass Transfer, 51(21-22), 5209-5225.

[23] Han, S., & Goldstein, R. J. (2008). The heat/mass transfer analogy for a simulated turbine endwall. International Journal of Heat and Mass Transfer, 51(11-12), 3227-3244.

[24] Ravelli, S., & Barigozzi, G. (2017). Comparison of RANS and Detached Eddy Simulation Modeling Against Measurements of Leading Edge Film Cooling on a First-Stage Vane. Journal of Turbomachinery, 139(5), 051005.

[25] Goldstein, R. J. (1971). Film cooling. In Advances in heat transfer (Vol. 7, pp. 321-379). Elsevier.

[26] https://www.engineeringtoolbox.com

[27] Winn, E. B. (1950). The temperature dependence of the self-diffusion coefficients of argon, neon, nitrogen, oxygen, carbon dioxide, and methane. Physical review, 80(6), 1024.

[28] ANSYS Fluent v. 18 Theory Guide.

[29] Ravelli, S., Barigozzi, G., Casartelli, E., & Mangani, L. (2017). Assessment of transition modeling and compressibility effects in a linear cascade of turbine nozzle guide vanes. Journal of Fluids Engineering, 139(5), 051104.

[30] Reynolds, O. (1883). XXIX. An experimental investigation of the circumstances which determine whether the motion of water shall he direct or sinuous, and of the law of resistance in parallel channels. Philosophical Transactions of the Royal Society of London, 174, 935-982.

Highlights

- Showerhead film cooling on a first-stage vane was numerically investigated
- The influence of *BR* and *DR* on leading edge adiabatic effectiveness was evaluated
- Coolant was air at different temperature from the mainstream or isothermal foreign gas
- The heat/mass transfer analogy was valid at the lowest blowing condition of $BR = 2$
- Its validity was extended to $BR = 3$, in case of $DR \sim 1.5$ and high mainstream turbulence